

Sparse Representation of Gravitational Sound

Laura Rebollo-Neira
Mathematics Department
Aston University
B3 7ET, Birmingham, UK

A. Plastino
IFLP-CCT-Conicet
National University of La Plata
CC 727, 1900 La Plata, Argentina

January 2, 2018

Abstract

Gravitational Sound clips produced by the Laser Interferometer Gravitational-Wave Observatory (LIGO) and the Massachusetts Institute of Technology (MIT) are considered within the particular context of data reduction. We advance a procedure to this effect and show that these types of signals can be approximated with high quality using *significantly fewer elementary components* than those required within the standard orthogonal basis framework. Furthermore, a local measure sparsity is shown to render meaningful information about the variation of a signal along time, by generating a set of local sparsity values which is much smaller than the dimension of the signal. This point is further illustrated by recourse to a more complex signal, generated by Milde Science Communication to divulge Gravitational Sound in the form of a ring tone.

Keywords: Gravitational Sound; Sparse Representation; Mixed Dictionary; Greedy Pursuit Strategy.

1 Introduction

In 1905 Henri Poincaré first suggested that accelerated masses in a relativistic field should produce gravitational waves [1]. The idea was magisterially pursued by Einstein via his celebrated theory of general relativity. In 1918 he published his famous quadrupole formula for gravitational radiation [2]. A century later, the LIGO Scientific Collaboration and Virgo Collaboration published a paper about the gravitational radiation they had detected on September 2015 [3]. Ever since scientists believe to have entered in a new era of astronomy, whereby the universe will be studied by ‘its sound’ [4–8]. Gravitational Sound (GS) signals will then be here scrutinized with advanced techniques.

In the signal processing field, the problem of finding a sparse approximation for a signal consists in expressing the signal as a superposition of as few elementary components as possible, without significantly affecting the quality of the reconstruction. In signal processing applications the approximation is carried out on a signal partition, i.e., by dividing the signal into small pieces and constructing the approximation for each of those pieces of data. Traditional techniques would carry out the task using an orthogonal basis. However, enormous improvements in sparsity can be achieved using an adequate over-complete ‘dictionary’ and an appropriate mathematics method. For the most part, these methods are based on minimization of the l_1 -norm [9] or are greedy pursuit strategies [10–18], the latter being much more effective in practice.

Sparse signal representation of sound signals is a valuable tool for a number of auditory tasks [19–21]. Vibration signal processing also benefits by sparsity constraints [22, 23]. Moreover, the emerging theory of compressive sensing [24–26] has enhanced the concept of sparsity by asserting that the number of measurements needed for accurate representation of a signal informational content decreases if the sparsity of the representation improves. Hence, when some GS tones made with the observed Gravitation Wave (GW) were released, we felt motivated to produce a sparse approximation of those clips.

We simply analyze the GS tones from a processing viewpoint, regardless on how and why they have been generated. We consider a) a short tone made with the chirp `gw151226` that has been detected, b) the theoretical simulated GS, `iota_20_10000_4_4_90_h`, and c) the `Black_Hole_Billiards` ring tone, which is a more complex signal produced by superposition with an ad hoc independent percussive sound. The ensuing results are certainly interesting. If, in the future, GS signals are to be generated at large scale (as astronomical images have been produced [27, 28]), it is important to have tools for all kinds of processing of those signals.

The central goal of this Communication is to present evidences of the significant gain in sparsity achieved if a GS signal is approximated with high quality outside the orthogonal basis framework. For demonstration purposes we have made available the MATLAB routines for implementation of the method.

1.1 Preliminary definitions and notation

The traditional frequency decomposition of a signal given by N sample points, $f(i)$, $i = 1, \dots, N$, involves the Fourier expansion

$$f(i) = \frac{1}{\sqrt{N}} \sum_{n=1}^M c(n) e^{i \frac{2\pi(i-1)(n-1)}{M}}, \quad i = 1, \dots, N.$$

The values $|c(n)|$, $n = 1, \dots, M = N$ are called the discrete Fourier spectrum of the signal, and can be evaluated in a very effective manner via the Fast Fourier Transform (FFT). For $M > N$ even if the coefficients in the above expansion can still be calculated via FFT, by zero padding, these are not longer unique. Finding a sparse solution is the goal of sparse approximation techniques.

The problem of the sparse approximation of a signal, outside the orthogonal basis setting, consists in using elements of a redundant set, called a *dictionary*, for constructing an approximation involving a number of elementary components which is significantly smaller than the signal dimension. For signals whose structure varies with time, sparsity performs better when the approximation is carried out on a signal partition. In order to give precise definitions we introduce at this point the notational usual conventions: \mathbb{R} and \mathbb{C} represent the sets of real and complex numbers, respectively. Boldface fonts are used to indicate Euclidean vectors and standard mathematical fonts to indicate components, e.g., $\mathbf{d} \in \mathbb{C}^N$ is a vector of N -components $d(i) \in \mathbb{C}^N$, $i = 1, \dots, N$. The operation $\langle \cdot, \cdot \rangle$ indicates the Euclidean inner product and $\|\cdot\|$ the induced norm, i.e. $\|\mathbf{d}\|^2 = \langle \mathbf{d}, \mathbf{d} \rangle$, with the usual inner product definition: For $\mathbf{d} \in \mathbb{C}^N$ and $\mathbf{f} \in \mathbb{C}^N$

$$\langle \mathbf{f}, \mathbf{d} \rangle = \sum_{i=1}^N f(i)d^*(i),$$

where $d^*(i)$ stands for the complex conjugate of $d(i)$.

A partition of a signal $\mathbf{f} \in \mathbb{R}^N$ is represented as a set of disjoint pieces, $\mathbf{f}_q \in \mathbb{R}^{N_b}$, $q = 1, \dots, Q$, henceforth to be called ‘blocks’, which, without loss of generality, are assumed to be all of the same size and such that $QN_b = N$. Denoting by $\hat{\mathbf{J}}$ the concatenation operator, the signal $\mathbf{f} \in \mathbb{R}^N$ is ‘assembled’ from the blocks as $\mathbf{f} = \hat{\mathbf{J}}_{q=1}^Q \mathbf{f}_q$. The concatenation operation $\hat{\mathbf{J}}$ is defined as follows: given $\mathbf{f}_1 \in \mathbb{R}^{N_b}$ and $\mathbf{f}_2 \in \mathbb{R}^{N_b}$, the vector $\mathbf{f} = \mathbf{f}_1 \hat{\mathbf{J}} \mathbf{f}_2$ is a vector in \mathbb{R}^{2N_b} having components $f(i) = f_1(i)$ for $i = 1, \dots, N_b$, and $f(i) = f_2(i - N_b)$ for $i = N_b + 1, \dots, 2N_b$. Thus, $\mathbf{f} = \hat{\mathbf{J}}_{q=1}^Q \mathbf{f}_q$ is a vector in \mathbb{R}^{QN_b} having components $f(i) = f_q(i - (q - 1)N_b)$, $i = (q - 1)N_b + 1, \dots, qN_b$, $q = 1, \dots, Q$. Consequently $\langle \mathbf{f}, \mathbf{f} \rangle = \|\mathbf{f}\|^2 = \sum_{q=1}^Q \|\mathbf{f}_q\|^2$.

A *dictionary* for \mathbb{R}^{N_b} is an *over-complete* set of (normalized to unity) elements $\mathcal{D} = \{\mathbf{d}_n \in \mathbb{R}^{N_b}; \|\mathbf{d}_n\| = 1\}_{n=1}^M$, which are called *atoms*.

2 Sparse Signal Approximation

Given a signal partition $\mathbf{f}_q \in \mathbb{R}^{N_b}$, $q = 1, \dots, Q$ and a dictionary \mathcal{D} , the k_q -term approximation for each block is given by an atomic decomposition of the form

$$\mathbf{f}_q^{k_q} = \sum_{n=1}^{k_q} c^{k_q}(n) \mathbf{d}_{\ell_n^q}, \quad q = 1, \dots, Q. \quad (1)$$

The approximation to the whole signal is then obtained simply by joining the approximation for the blocks as $\mathbf{f}^K = \hat{\mathbb{J}}_{q=1}^Q \mathbf{f}_q^{k_q}$, where $K = \sum_{q=1}^Q k_q$.

2.1 The Method

The problem of finding the minimum number of K terms such that $\|\mathbf{f} - \mathbf{f}^K\| < \rho$, for a given tolerance parameter ρ , is an NP-hard problem [12]. In practical applications, one looks for tractable sparse solutions. For this purpose we consider the Optimized Hierarchical Block Wise (OHBW) version [29] of the Optimized Orthogonal Matching Pursuit (OOMP) [13] approach. This entails that, in addition to selecting the dictionary atoms for the approximation of each block, the blocks are ranked for their sequential stepwise approximation. As a consequence, the approach is optimized in the sense of minimizing, at each iteration step, the norm of the total residual error $\|\mathbf{f} - \mathbf{f}^K\|$ [29]. As will be illustrated in Sec. 2.3, when approximating a signal with pronounced amplitude variations the sparsity result achieved by this strategy is remarkable superior to that arising when the approximation of each block is completed at once, i.e., when the ranking of blocks is omitted. The OHBW-OOMP method is implemented using the steps indicated below.

OHBW-OOMP Algorithm

- 1) For $q = 1, \dots, Q$ initialize the algorithm by setting: $\mathbf{r}_q^0 = \mathbf{f}_q$, $\mathbf{f}_q^0 = 0$, $\Gamma_q = \emptyset$, $k_q = 0$, and selecting the ‘potential’ first atom for the atomic decomposition of every block q as the one corresponding to the indexes ℓ_1^q such that

$$\ell_1^q = \arg \max_{n=1, \dots, M} |\langle \mathbf{d}_n, \mathbf{r}_q^{k_q} \rangle|^2, \quad q = 1, \dots, Q. \quad (2)$$

Assign $\mathbf{w}_1^q = \mathbf{b}_1^q = \mathbf{d}_{\ell_1^q}$.

- 2) Use the OHBW criterion for selecting the block to upgrade the atomic decomposition by adding one atom

$$q^* = \arg \max_{q=1, \dots, Q} \frac{|\langle \mathbf{w}_{k_q+1}^q, \mathbf{f}_q \rangle|^2}{\|\mathbf{w}_{k_q+1}^q\|^2}. \quad (3)$$

If $k_{q^*} > 0$ upgrade vectors $\{\mathbf{b}_n^{k_{q^*}, q^*}\}_{n=1}^{k_{q^*}}$ for block q^* as

$$\begin{aligned} \mathbf{b}_n^{k_{q^*}+1, q^*} &= \mathbf{b}_n^{k_{q^*}, q^*} - \mathbf{b}_{k_{q^*}+1}^{k_{q^*}+1, q^*} \langle \mathbf{d}_{\ell_{k_{q^*}+1}^{q^*}}, \mathbf{b}_n^{k_{q^*}+1, q^*} \rangle, \quad n = 1, \dots, k_{q^*}, \\ \mathbf{b}_{k_{q^*}+1}^{k_{q^*}+1, q^*} &= \frac{\mathbf{w}_{k_{q^*}+1}^{q^*}}{\|\mathbf{w}_{k_{q^*}+1}^{q^*}\|^2}. \end{aligned} \quad (4)$$

3) Calculate

$$\begin{aligned}\mathbf{r}_{q^*}^{k_{q^*}+1} &= \mathbf{r}_{q^*}^{k_{q^*}} - \langle \mathbf{w}_{k_{q^*}+1}^{q^*}, \mathbf{f}_{q^*} \rangle \frac{\mathbf{w}_{k_{q^*}+1}^{q^*}}{\|\mathbf{w}_{k_{q^*}+1}^{q^*}\|^2}, \\ \mathbf{f}_{q^*}^{k_{q^*}+1} &= \mathbf{f}_{q^*}^{k_{q^*}+1} + \langle \mathbf{w}_{k_{q^*}+1}^{q^*}, \mathbf{f}_{q^*} \rangle \frac{\mathbf{w}_{k_{q^*}+1}^{q^*}}{\|\mathbf{w}_{k_{q^*}+1}^{q^*}\|^2}.\end{aligned}\quad (5)$$

Upgrade the set $\Gamma_{q^*} \leftarrow \Gamma_{q^*} \cup \ell_{k_{q^*}+1}$ and increase $k_{q^*} \leftarrow k_{q^*} + 1$.

4) Select a new potential atom for the atomic decomposition of block q^* , using the OOMP criterion, i.e., choose $\ell_{k_{q^*}+1}^{q^*}$ such that

$$\ell_{k_{q^*}+1}^{q^*} = \arg \max_{\substack{n=1,\dots,M \\ n \notin \Gamma_{q^*}}} \frac{|\langle \mathbf{d}_n, \mathbf{r}_{q^*}^{k_{q^*}} \rangle|^2}{1 - \sum_{i=1}^{k_{q^*}} |\langle \mathbf{d}_n, \tilde{\mathbf{w}}_i^{q^*} \rangle|^2}, \quad \text{with} \quad \tilde{\mathbf{w}}_i^{q^*} = \frac{\mathbf{w}_i^{q^*}}{\|\mathbf{w}_i^{q^*}\|}, \quad (6)$$

5) Compute the corresponding new vector $\mathbf{w}_{k_{q^*}+1}^{q^*}$ as

$$\mathbf{w}_{k_{q^*}+1}^{q^*} = \mathbf{d}_{\ell_{k_{q^*}+1}^{q^*}}^{q^*} - \sum_{n=1}^{k_{q^*}} \frac{\mathbf{w}_n^{q^*}}{\|\mathbf{w}_n^{q^*}\|^2} \langle \mathbf{w}_n^{q^*}, \mathbf{d}_{\ell_{k_{q^*}+1}^{q^*}}^{q^*} \rangle. \quad (7)$$

including, for numerical accuracy, the re-orthogonalizing step:

$$\mathbf{w}_{k_{q^*}+1}^{q^*} \leftarrow \mathbf{w}_{k_{q^*}+1}^{q^*} - \sum_{n=1}^{k_{q^*}} \frac{\mathbf{w}_n^{q^*}}{\|\mathbf{w}_n^{q^*}\|^2} \langle \mathbf{w}_n^{q^*}, \mathbf{w}_{k_{q^*}+1}^{q^*} \rangle. \quad (8)$$

6) Check if, for a given K and ρ either the condition $\sum_{q=1}^Q k_q = K+1$ or $\|\mathbf{f} - \mathbf{f}^K\| < \rho$ has been met.

If that is the case, for $q = 1, \dots, Q$ compute the coefficients $c^{k_q}(n) = \langle \mathbf{b}_n^{k_q}, \mathbf{f}_q \rangle$, $n = 1, \dots, k_q$.

Otherwise repeat steps 2) - 5).

Remark 1: For all the values of q , the OOMP criterion (6) in the algorithm above ensures that, fixing the set of previously selected atoms, the atom corresponding to the indexes given by (6) minimizes the local residual norm $\|\mathbf{f}_q - \mathbf{f}_q^{k_q}\|$ [13]. That is why in one of the earliest references [30] is called Orthogonal Least Square. In our context the term OOMP also refers to the particular implementation. Moreover, the OHBW-OOMP criterion (3) for choosing the block to upgrade the approximation, ensures the minimization of the total residual norm [29]. Let us recall that the OOMP approach optimizes the Orthogonal Matching Pursuit (OMP) one [11]. The latter is also an optimization of the plain Matching Pursuit (MP) method [10](see the discussion in [13]).

2.2 The Dictionary

The degree of success in achieving high sparsity using a dictionary approach depends on both, the suitability of the mathematical method for finding a tractable sparse solution and the dictionary itself. As in the case of melodic music [29,31], we found the trigonometric dictionary \mathcal{D}_T , which is the union of the dictionaries \mathcal{D}_C and \mathcal{D}_S given below, to be an appropriate dictionary for approximating these GS signals.

$$\begin{aligned}\mathcal{D}_C^x &= \{w_c(n) \cos \frac{\pi(2i-1)(n-1)}{2M}, i = 1, \dots, N_b\}_{n=1}^M \\ \mathcal{D}_S^x &= \{w_s(n) \sin \frac{\pi(2i-1)(n)}{2M}, i = 1, \dots, N_b\}_{n=1}^M.\end{aligned}$$

In the above sets $w_c(n)$ and $w_s(n)$, $n = 1, \dots, M$ are normalization factors.

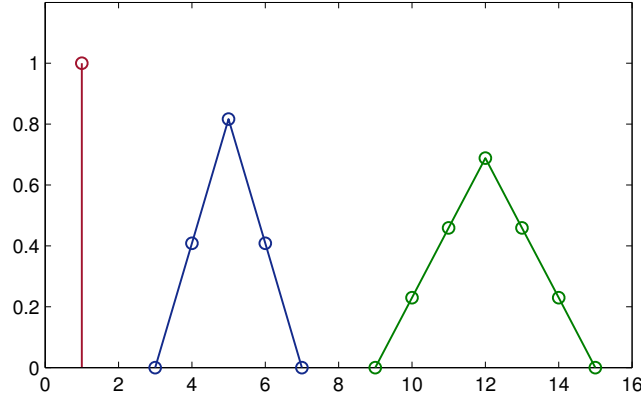


Figure 1: Prototype atoms \mathbf{p}_1 , \mathbf{p}_2 and \mathbf{p}_3 , which generate the dictionaries \mathcal{D}_{P_1} , \mathcal{D}_{P_2} and \mathcal{D}_{P_3} by sequential translations of one point.

Since a GS tone is characterized by ending in a sharp rise, we have found that a sparse model benefits by the inclusion of a dictionary constructed by translation of the prototype atoms, \mathbf{p}_1 , \mathbf{p}_2 and \mathbf{p}_3 in Fig. 1. This type of dictionary is inspired by a general result holding for continuous spline spaces. Namely, that spline spaces on a compact interval can be spanned by dictionaries of B-splines of broader support than the corresponding B-spline basis functions [32,33]. Thus, the prototypes in Fig. 1 are generated using linear B-spline functions of different support. For $m = 1, 2, 3$, they are defined as follows:

$$p_m(x) = \begin{cases} \frac{x}{m} & \text{if } 0 \leq x < m \\ 2 - \frac{x}{m} & \text{if } m \leq x < 2m \\ 0 & \text{otherwise.} \end{cases} \quad (9)$$

The corresponding dictionaries \mathcal{D}_{P_1} , \mathcal{D}_{P_2} and \mathcal{D}_{P_3} are created by discretization of the variable x in

(9) and sequential translation of one sampling point, i.e.,

$$\mathcal{D}_{P_n} = \{b_i p_m(j-i)|N_b; j = 1, \dots, N_b\}_{i=1}^M, \quad m = 1, 2, 3$$

where the notation $p_m(j-i)|N_b$ indicates the restriction to be an array of size N_b . The numbers b_i , $i = 1, \dots, M$ are normalization factors.

The dictionary \mathcal{D}_P consisting of atoms of different support is built by merging \mathcal{D}_{P_1} , \mathcal{D}_{P_2} and \mathcal{D}_{P_3} as $\mathcal{D}_P = \mathcal{D}_{P_1} \cup \mathcal{D}_{P_2} \cup \mathcal{D}_{P_3}$. The whole mixed dictionary is then $\mathcal{D}_M = \mathcal{D}_T \cup \mathcal{D}_P$, with $\mathcal{D}_T = \mathcal{D}_C \cup \mathcal{D}_S$. Interestingly enough, the dictionary \mathcal{D}_M happens to be a sub-dictionary of a larger dictionary proposed in [34] for producing sparse representations of astronomical images. The difference being that, in this case, sparsity does not improve in a significant way by further enlarging the dictionary.

From a computational viewpoint the particularity of the sub-dictionaries \mathcal{D}_C and \mathcal{D}_S is that the inner product with all its elements can be evaluated via FFT. This possibility reduces the complexity of the numerical calculations when the partition unit N_b is large [29, 31]. Also, the inner products with the atoms of the dictionaries \mathcal{D}_{P_2} and \mathcal{D}_{P_3} can be effectively implemented, all at once, via a convolution operation.

Note: The MATLAB routine implementing the OHBW-OOMP approach, dedicated to the dictionary introduced in this section, has been made available on [35].

2.3 The Processing

We process now the three signals we are considering here:

- a) The audio representation of the detected `gw151226` chirp [36].
- b) The tone of the theoretical gravitational wave `iota_20_10000_4_4_90_h` [37].
- c) The `Black_Hole_Billiards` ring tone [36].

The quality of an approximation is measured by the Signal to Noise Ratio (SNR) which is defined as

$$\text{SNR} = 10 \log_{10} \frac{\|\mathbf{f}\|^2}{\|\mathbf{f} - \mathbf{f}^K\|^2} = 10 \log_{10} \frac{\sum_{q=1}^{N_b, Q} |f_q(i)|^2}{\sum_{q=1}^{N_b, Q} |f_q(i) - f_q^{k_q}(i)|^2}. \quad (10)$$

The sparsity of the whole representation is measured by the Sparsity Ratio (SR) defined as $\text{SR} = \frac{N}{K}$, where K is the total number of coefficients in the signal representation defined above.

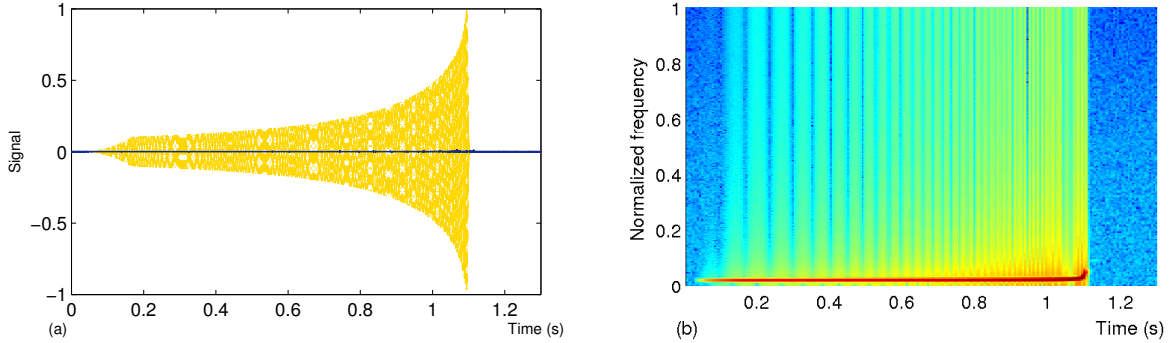


Figure 2: (a) represents the clip `gw151226`. The central dark line is the residual error of the approximation, up to SNR=50dB. (b) is the classic spectrogram of the clip in (a).

Audio representation of the chirp `gw151226`

This clip, made with the detected short chirp `gw151226`, is plotted in the graph (a) of Fig.2. It consists of $N = 65536$ samples. Graph (b) is its classic spectrogram.

When a trigonometric orthogonal basis for approximating this signal is used, the best sparsity result is achieved with the Discrete Cosine Transform (DCT). Hence, we first approximate the clip, up to SNR=50dB, by nonlinear thresholding of the DCT coefficients. As in the case of the dictionary approach, the approximation with DCT is carried out following two different strategies. One of the strategies is identical to the OOMP one, but involves a straightforward implementation due to the orthogonality property of DCT. For each block, only the k_q DCT coefficients of largest magnitude are kept. Each k_q value is determined by requesting an approximation of each block up to SNR=50dB. We term this strategy the nonlinear DCT (NL-DCT) approximation. The other strategy selects the DCT components in a OHBW manner to construct an approximation, up to SNR=50dB, as described in Sec. 2.1. The implementation is much simpler though, due to the orthogonality of DCT. We refer to this method as OHBW-NL-DCT. The results of the achieved SR, for both DCT-based strategies are given in the second and third columns of Table 1 for different values of N_b . The fourth and fifth columns of the table show the SR values for the OOMP and OHBW-OOMP approaches, respectively, using the dictionary \mathcal{D}_M given in Sec. 2.2. As can be observed in Table 1, the highest SR is obtained for $N_b = 2048$ with the dictionary \mathcal{D}_M and applying the OHBW-OOMP method. However, while with the dictionary the SR decreases for $N_b = 4096$, the DCT results improve. Since the DCT does not generate memory problems when increasing the value of N_b , we have augmented this value until the maximum possible number was reached i.e. $N_b = N = 65536$. The conclusion of the study is that for $N_b = N = 65536$ the DCT secures its best performance. Nevertheless the best DCT result is still very poor (SR=28.7) in comparison to the results obtained with both methods

using the dictionary \mathcal{D}_M . Notice that for $N_b = 2048$ the dictionary approximation renders $\text{SR}=260.06$ with the OHBW-OOMP method and $\text{SR}=207.40$ with the OOMP one. Both values represent an enormous improvement of sparsity in relation to the best DCT result.

N_b	NL-DCT	OHBW-NL-DCT	OOMP	OHBW-OOMP
256	6.46	8.26	50.83	66.80
512	7.39	10.08	74.10	122.04
1024	9.02	11.96	126.51	206.08
2048	11.76	15.44	207.40	260.06
4096	12.51	18.93	107.01	253.03

Table 1: Comparison of the SRs produced by the DCT and dictionary approaches vs the length of the partition unit N_b .

Theoretical Gravitational Wave Sound

This is the `iota_20_10000_4_4_90_h` gravitational wave, which belongs to the family of Extreme Mass Ratio Inspirals [38–43] available on [37]. It consists of $N = 458752$ data points plotted in graph (a) of Fig. 3. The SRs obtained in the same way as for the previous clip are shown in Table 2.

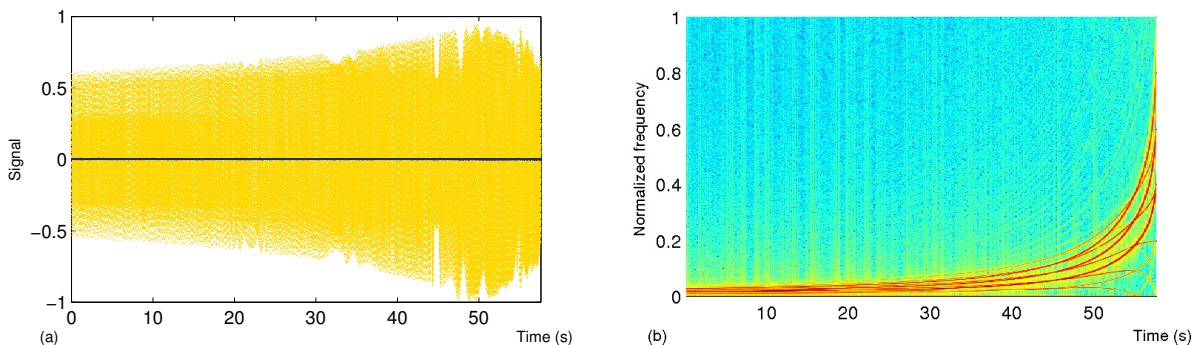


Figure 3: (a) represents the `iota_20_10000_4_4_90_h` tone. The central dark line is the residual error of the approximation, up to $\text{SNR}=50\text{dB}$. (b) is the classic spectrogram of the clip in (a).

Also in this case the best sparsity result with the dictionary approach occurs for $N_b = 2048$. By increasing the value of N_b the best DCT results ($\text{SR}=5.1$) is obtained with $N_b = 16384$ and is less than half of the value of the best SR produced by the dictionary approach ($\text{SR}=11.92$). Since the amplitude of the signal does not vary much along time, the SR obtained by approximating each block at once, with OOMP, does not significantly differ from the values obtained applying the OHBW-OOMP method. The same feature is observed by comparing the NL-DCT and OHBW-NL-DCT results.

N_b	NL-DCT	OHWB-NL-DCT	OOMP	OHBW-OOMP
256	2.77	2.81	7.40	7.57
512	3.22	3.25	9.00	9.14
1024	3.60	3.61	10.47	10.70
2048	3.96	3.98	11.59	11.92
4096	4.39	4.39	11.45	11.73

Table 2: Comparison of the SRs produced by the DCT and dictionary approaches, vs the length of the partition unit N_b , for the `iota_20_10000_4_4_90_h` clip.

The Black_Hole_Billiards ring tone

In order to stress the relevance of the technique for representing features of more complex signals by means of a very reduced set of points, we consider here the `Black_Hole_Billiards` ring tone available on [36]. This clip was created by Milde Science Communication by superimposing a sound of percussive nature (the billiards sound) to a GW chirp. It consists of $N = 262144$ samples plotted in graph (a) of Fig. 4. Graph (b) is its classic spectrogram.

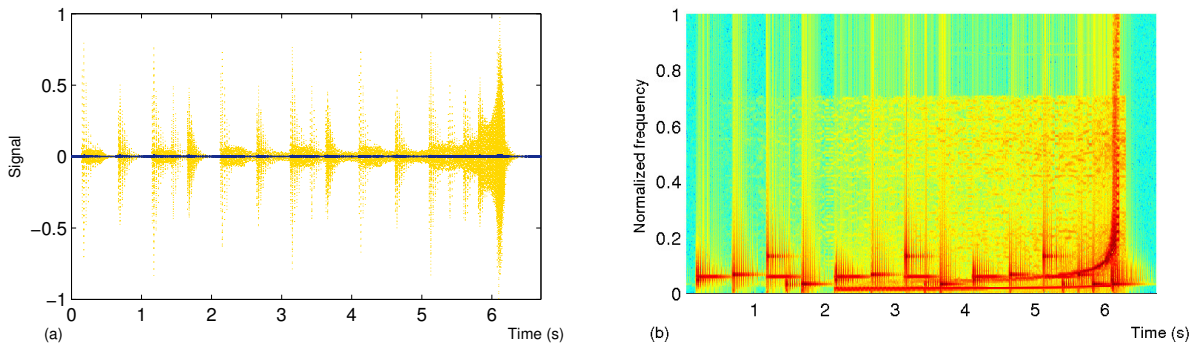


Figure 4: (a) represents the `Black_Hole_Billiards` clip. Credit: Milde Science Communication. The central dark line is the residual of the approximation, up to SNR=40dB. (b) is the spectrogram of the clip in (a).

For this signal the approximation is carried out up to SNR=40dB. The central dark line in graph (a) of Fig. 4 represents the difference between the signal and its approximation. The sparsity result are given in Table 3, from where it appears that the best dictionary result occurs for $N_b = 512$ with the OHWB-OOMP method, and the best DCT results occurs for $N_b = 2048$ with the OHWB-NL-DCT approach. As in the previous cases, the NL-DCT result improves by increasing the value of N_b . The best result (SR= 4.2) takes place for $N_b = 16384$, but is still smaller than the SR yielded by OHWB-NL-DCT (SR=6.31). Notice that the latter is not too far from the best result yielded by OOMP using the dictionary (SR=7.09) but less than half of the value obtained using the dictionary and the OHWB-OOMP approach (SR=13.82). This outcomes highlights the importance of adopting

the OHBW strategy for constructing the signal approximation when, as in this example, the signal amplitude varies significantly along the domain of definition.

N_b	NL-DCT	OHWB-NL-DCT	OOMP	OHBW-OOMP
256	3.07	5.67	6.75	12.92
512	3.34	6.12	6.80	13.82
1024	3.55	6.30	6.84	13.24
2048	3.62	6.31	6.78	12.81
4096	3.83	6.08	7.09	12.20

Table 3: Comparison of the SRs produced by the DCT and dictionary approaches, vs the length of the partition unit N_b , for the `Black_Hole_Billiards` clip.

2.4 The Role of Local Sparsity

The SR is a global measure of sparsity indicating the number of elementary components contained in the whole signal. An interesting description of the signal variation is rendered by a local measure of sparsity. For this we consider the local sparsity ratio $sr(q) = \frac{N_b}{k_q}$, $q = 1, \dots, Q$ where, as defined above, k_q is the number of coefficients in the decomposition of the q -block and N_b the size of the block.

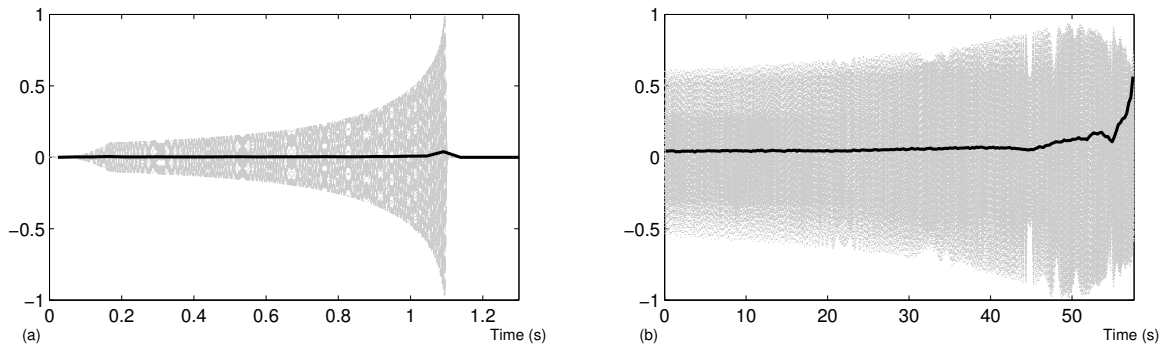


Figure 5: The dark line in (a) joins the inverse local sparsity values for the clip `gw151226`. (b) has the same description but for the `iota_20_10000_4_4_90_h` clip tone.

For illustration's convenience the darker lines in both graphs of Fig. 5 depict the inverse of this local measure by joining the values $1/sr(q)$, $q = 1, \dots, Q$. Each of these values is located in the horizontal axis at the center of the corresponding block and provides much information about the signal. Certainly, simply from the observation of the the darker line graph (a) of Fig. 5 (joining 32 points of inverse local sparsity ratio for $N_b = 2048$) one can realize that the number of internal components in the clip `gw151226` is roughly constant along the audible part of the signal, with a

relatively higher value only at the very end of this part. In the case of the `iota_20_10000_4_4_90_h` clip (graph (b) in the same figure) the line joining the 224 points of the inverse local sparsity ratio, for $N_b = 2048$, indicates a clear drop of sparsity towards the end of the signal, where the rapid rise of the tone does occur (c.f. spectrogram in Fig. 3 (b)).

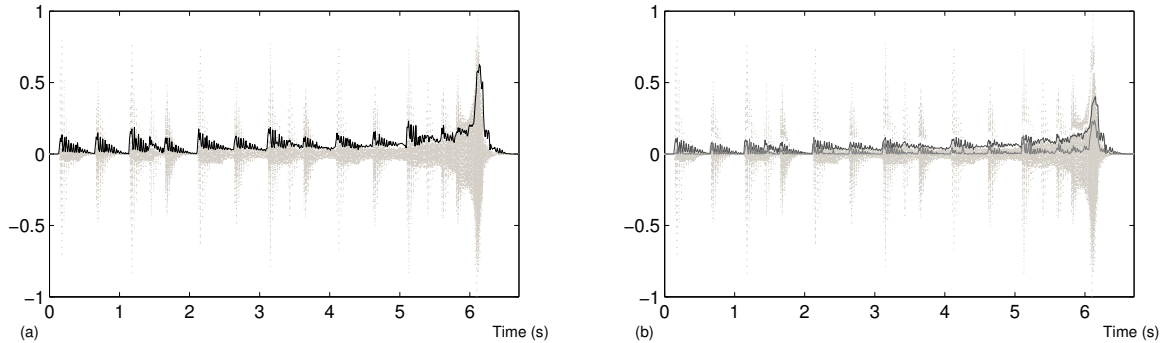


Figure 6: The darker line in (a) joins the inverse local sparsity ratio values for the `Black_Hole_Billiards` ring tone. The darker lines in (b) discriminate the inverse local sparsity ratio produced with atoms in the dictionary \mathcal{D}_P (from bottom to top the first line) and in the dictionary \mathcal{D}_T (next line).

Since the `Black_Hole_Billiards` ring tone is a more complex signal, due to the superposition of the artificial sound, the information given by the local sparsity ratio is richer than in the previous cases. Notice for instance that the darker line in graph (a) of Fig. 6 clearly indicates the offsets in the percussive part of the clip which has been superimposed to the GS chirp. Moreover this line, joining 512 points of inverse local sparsity ratio (for $N_b = 512$) also roughly follows the signal variation envelop. Graph (b) discriminates the local sparsity corresponding to atoms in the trigonometric component of the dictionary, and those in the dictionary \mathcal{D}_P . The first line (from bottom to top) represents the inverse local sparsity values corresponding to atoms in \mathcal{D}_P and the next line to atoms in \mathcal{D}_T . In this clip 20% of atoms are from dictionary \mathcal{D}_P and, as indicated in the graph (b) of Fig. 6, a significant contribution of those atoms takes place within the blocks where the rapid rise of the GS tone takes place (c.f. spectrogram in Fig. 4 (b)). Equivalently, for the clip in Fig. 3 17.9% of the atoms belongs to the dictionary \mathcal{D}_P . For the clip of Fig. 2, however, only 2.7% of the atoms comes from the to dictionary \mathcal{D}_P . This is due to the fact that, unlike the signals in Fig.3 and Fig. 4, the clip in Fig. 2 does not exhibit a major leap in its spectrogram.

3 Conclusions

We have here advanced an effective technique for the numerical representation of Gravitational Sound clips produced by the Laser Interferometer Gravitational-Wave Observatory (LIGO) and the Massachusetts Institute of Technology (MIT). The technique is inscribed within the particular context of sparse representation and data reduction. We laid out a procedure to this effect and were able to show that these types of signals can be approximated with high quality using *significantly fewer elementary components* than those required within the standard orthogonal basis framework. A local measure of sparsity has been shown to produce meaningful information about the signal internal variations along time. This information is contained in a set of points which is much smaller than the length of the signal.

Acknowledgments

Thanks are due to LIGO, MIT and Milde Science Communications for making available the GS tones we have used in this paper. We are particularly grateful to Prof. S. A. Hughes and Prof. B. Schutz, for giving us information on the generation of those signals. We are also appreciative to the anonymous Reviewers for their comments and suggestions to improve the presentation of the material.

References

- [1] J. L. Cervantes-Cota, S., Galindo-Uribarri, and G. F. Smoot, “A Brief History of Gravitational Waves”, *Universe* (2016) 2(3), 22; doi:10.3390/universe2030022.
- [2] A. Einstein, “Über Gravitationswellen” (“On Gravitational Waves”) In: *Sitzungsberichte der Kniglich Preussischen Akademie der Wis-senschaften Berlin* (1918), 154–167.
- [3] B. P. Abbott et al. (LIGO Scientific Collaboration and Virgo Collaboration), *Phys. Rev Lett.* 116, 061102 (2016), DOI: 10.1103/PhysRevLett.116.061102
- [4] B.P. Abbott et al. (LIGO Scientific Collaboration and Virgo Collaboration) “Binary Black Hole Mergers in the First Advanced LIGO Observing Run”, *Phys. Rev. X*, **6**, 041015, (2016)
- [5] B.P. Abbott et al. (LIGO Scientific Collaboration and Virgo Collaboration), “B.P. Abbott et al. (LIGO Scientific Collaboration and Virgo Collaboration), “Properties of the Binary

- Black Hole Merger GW150914”, *Phys. Rev. Lett.* **116**, 241102 (2016), DOI: 10.1103/PhysRevLett.116.241102.
- [6] K. Belczynski, D. E. Holz, T Bulik, and R. O’Shaughnessy, “The first gravitational-wave source from the isolated evolution of two stars in the 40100 solar mass range”, *Nature*, **534**, 512–515 (2016) doi:10.1038/nature18322.
- [7] N. Yunes, K. Yagi, and F. Pretorius, “Theoretical physics implications of the binary black-hole mergers GW150914 and GW151226”, *Phys. Rev. D*, **94**, 084002 (2016).
- [8] R. M. O’Leary, Y. Meiron, and B. Kocsis, “Dynamical formation signatures of black hole binaries in the first detected mergers by LIGO”, *Astrophysical Journal Letters*, **824**, 1–L12 (2016).
- [9] S. S. Chen, D. L. Donoho, and M. A Saunders, “Atomic Decomposition by Basis Pursuit”, *SIAM Journal on Scientific Computing*, **20**, 33–61 (1998).
- [10] S. Mallat and Z. Zhang, “Matching pursuit with time-frequency dictionaries,” *IEEE Transactions on Signal Processing*, **41**, 3397–3415 (1993).
- [11] Y.C. Pati, R. Rezaifar, and P.S. Krishnaprasad, “Orthogonal matching pursuit: recursive function approximation with applications to wavelet decomposition,” *Proc. of the 27th ACSSC*, **1**, 40–44 (1993).
- [12] B. K. Natarajan, “Sparse Approximate Solutions to Linear Systems”, *SIAM Journal on Computing*, **24**, 227–234 (1995).
- [13] L. Rebollo-Neira and D. Lowe, “Optimized orthogonal matching pursuit approach”, *IEEE Signal Process. Letters*, **9**, 137–140 (2002)
- [14] M. Andrieu, L. Rebollo-Neira, and E. Sagonos, “Backward-optimized orthogonal matching pursuit approach”, *IEEE Signal Process. Let.*, **11**, 705–708 (2004).
- [15] M. Andrieu and L. Rebollo-Neira, “A swapping-based refinement of orthogonal matching pursuit strategies”, *Signal Processing*, **86**, 480–495 (2006).
- [16] J. A. Tropp, “Greed is good: algorithmic results for sparse approximation”, *IEEE Transactions on Information Theory*, **50**, 2231–2242 (2004).
- [17] D. L. Donoho, Y. Tsaig, I. Drori, and J. Starck, “Stagewise Orthogonal Matching Pursuit”, *IEEE Transactions on Information Theory*, **58**, 1094–1121 (2006).

- [18] D. Needell and J.A. Tropp, “CoSaMP: Iterative signal recovery from incomplete and inaccurate samples”, *Applied and Computational Harmonic Analysis*, **26**, 301–321 (2009).
- [19] E. C. Smith, M. S. Lewicki, “Efficient auditory coding,” *Nature*, **439**, no. 7079, pp. 978982, 2006
- [20] J. Nam, J. Herrera, M. Slaney, and J. Smith, “Learning sparse feature representations for music annotation and retrieval,” in Proc. ISMIR , 2012.
- [21] M. D. Plumbley, T. Blumensath, L. Daudet, R. Gribonval, and M. E. Davies, “Sparse representations in audio and music: From coding to source separation,” *Proc. IEEE*, **98**, 995–1005 (2010).
- [22] Qiao B., Zhang X., Wang C., Zhang H., Chen X., “Sparse regularization for force identification using dictionaries”, *Journal of Sound and Vibration*, **368**, 71–86 (2016).
- [23] Qiao B, Zhang X, Gao J, Chen X. “Impact-force sparse reconstruction from highly incomplete and inaccurate measurements”. *Journal of Sound and Vibration*,**376**, 72–94 (2016).
- [24] D. L. Donoho, “Compressed sensing”, *IEEE Transactions on Information Theory*, **52**, 1289 – 1306 (2006).
- [25] E. Candès and M. Wakin, “An introduction to compressive sampling”, *IEEE Signal Processing Magazine*, **25**, 21 – 30 (2008).
- [26] R. Baraniuk, “More Is less: Signal processing and the data deluge”, *Science*, **331**, 717 – 719 (2011).
- [27] <http://http://www.eso.org/public/>
- [28] <http://hubblesite.org/>
- [29] L. Rebollo-Neira, “Cooperative greedy pursuit strategies for sparse signal representation by partitioning”, *Signal Processing*, **125**, 365–375 (2016).
- [30] S. Chen, S. A. Billings, W. Luo, “Orthogonal least squares methods and their application to non-linear system identification”, *International Journal of Control*, **50**, 1873 – 1896 (1989).
- [31] L. Rebollo-Neira, G. Aggarwal, “A dedicated greedy pursuit algorithm for sparse spectral representation of music sound”, *Journal of The Acoustic Society of America*, **140**, 2933 (2016).

- [32] M. Andrie, L. Rebollo-Neira, “Cardinal B-spline dictionaries on a compact interval,” *Applied and Computational Harmonic Analysis*, **18**, 336–346 (2005).
- [33] L. Rebollo-Neira, Z. Xu, “Adaptive non-uniform B-spline dictionaries on a compact interval”, *Signal Processing*, doi:10.1016/j.sigpro.2010.02.004, 2010.
- [34] L. Rebollo-Neira, J. Bowley “Sparse representation of astronomical images”, *Journal of The Optical Society of America A*, **30**, 758–768 (2013).
- [35] <http://www.nonlinear-approx.info/examples/node05.html>
- [36] <http://www.ligo.org/multimedia>
- [37] http://gmunu.mit.edu/sounds/emri_sounds/a0.998/a0.998.html
- [38] S. A. Hughes, “The evolution of circular, non-equatorial orbits of Kerr black holes due to gravitational-wave emission”, *Phys. Rev. D*, **61**, 084004 (2000).
- [39] S. A. Hughes, “Evolution of circular, non-equatorial orbits of Kerr black holes due to gravitational-wave emission: II. Inspiral trajectories and gravitational waveforms”, *Phys. Rev. D*, **64**, 064004 (2001).
- [40] K. Glampedakis, S. A. Hughes, D. Kennefick, “Approximating the inspiral of test bodies into Kerr black holes”, *Phys. Rev. D*, **66**, 064005 (2002).
- [41] L. Barack, C Cutler, “LISA capture sources: Approximate Waveforms, Signal-to-Noise Ratios, and Parameter Estimation Accuracy”, *Phys. Rev. D*, **69**, 082005 (2004).
- [42] S. A. Hughes, S. Drasco, E. E. Flanagan, J. Franklin, “Gravitational radiation reaction and inspiral waveforms in the adiabatic limit, *Phys. Rev. Lett.* **94**, 221101 (2005).
- [43] S. Drasco and S. A. Hughes, “Gravitational wave snapshots of generic extreme mass ratio inspirals”, *Phys. Rev. D*, **73**, (2006).